NANO LETTERS

Letter

pubs.acs.org/NanoLett

Vertical Graphene-Base Hot-Electron Transistor

Caifu Zeng,[†] Emil B. Song,[†,‡] Minsheng Wang,[†] Sejoon Lee,[†,§] Carlos M. Torres, Jr.,[†] Jianshi Tang,[†] Bruce H. Weiller,[‡] and Kang L. Wang*[,†]

[†]Department of Electrical Engineering, University of California, Los Angeles, California 90095, United States

[‡]The Aerospace Corporation, Los Angeles, California 90009, United States

[§]Quantum-Functional Semiconductor Research Center, Dongguk University-Seoul, Seoul 100-715, Korea

Supporting Information

ABSTRACT: We demonstrate vertical graphene-base hot-electron transistors (GB-HETs) with a variety of structures and material parameters. Our GB-HETs exhibit a current saturation with a high current on−off ratio (>10^5), which results from both the vertical transport of hot electrons across the ultrathin graphene base and the filtering of hot electrons through a built-in energy barrier. The influences of the materials and their thicknesses used for the tunneling and filtering barriers on the common-base current gain α are studied. The optimization of the SiO_2 thickness and using HfO_2 as the filtering barrier significantly improves the common-base current gain α by more than 2 orders of magnitude. The results demonstrate that GB-HETs have a great potential for high-frequency, high-speed, and high-density integrated circuits.

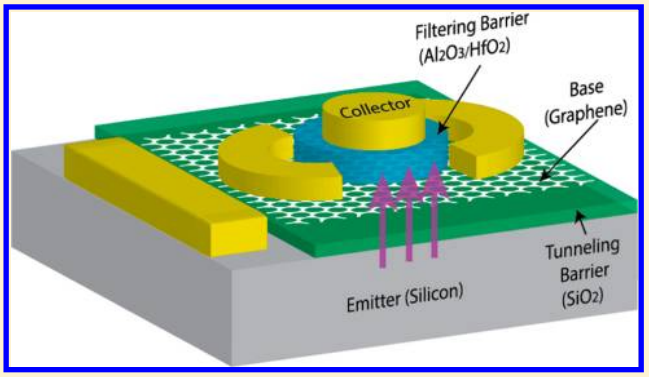

KEYWORDS: *Graphene, hot electron transistor, graphene base, graphene heterostructure, on−off ratio, current gain*

Graphene has garnered much attention for its unique physical properties. The high mobility, two-dimensional (2D) structure, and large-scale production[1−3] make it attractive for high-speed electronic devices. The field-effect transistors with graphene channels (GFETs) have shown a high cutoff frequency of several hundred gigahertz,[4,5] however, the channel mobility in GFETs is still limited from various extrinsic scattering sources,[6,7] and the unsatisfying saturation behavior degrades the device performance of GFETs, for example, a lowering of the cutoff frequency, decrease in the intrinsic gain and other figures of merit.[8] In addition, GFETs cannot be completely switched off because of the absence of a bandgap in graphene, and hence they are unsuitable for high-speed digital logic applications.

In the past, hot-electron transistors (HETs) have also been investigated as a promising candidate for high-speed electronic devices because of their short base transit time.[9−13] However, because of the shortfall in material selections and fabrication technology, most HETs investigated previously suffer from difficulties in further reducing the base thickness in order to achieve a short transit time and a high gain while maintaining a low base series resistance.[14,15] To overcome these obstacles, the concept of using graphene as the base region for hot-electron transistors (GB-HET) has been proposed by Mehr et al.,[16] followed by Kong et al.[17] The GB-HET utilizes both the operational principle of conventional HETs and the unique properties of graphene (e.g., the single atomic thickness, and the semimetallic property). These properties positively influence the base transit time and the base series resistance, which can improve device performances for high-speed and high-frequency applications.[16,17] Prototypes of GB-HETs have been fabricated and tested to illustrate the device concept recently.[18] However, these prototypes still suffered from poor isolation between the output and input terminals (e.g., the lack of the current saturation behavior in the output characteristics) and low common-base current gain, α.

In this Letter, we fabricate four types of GB-HETs and successfully demonstrate their operation. The device parameters that may affect α (e.g., the materials and their thicknesses for the tunneling and filtering barriers) have been studied. By optimizing the device parameters, it is shown that α can be significantly improved. Current saturation with high on−off ratio is observed in the output characteristics of our GB-HETs. We thoroughly analyze the device characteristics and explain them in detail.

A schematic diagram of the structure of our first type of GB-HET (D1) is shown in Figure 1a,b, where the silicon, graphene, and metal are used as the emitter, base, and collector, respectively. The SiO_2 layer serves as the tunneling barrier and the Al_2O_3 layer serves as the filtering barrier. The fabrication starts with growing an 8 nm thick thermal SiO_2 on top of a degenerately doped Si substrate ($n \sim 1 \times 10^{19}$

Received: December 8, 2012
Revised: May 10, 2013

dx.doi.org/10.1021/nl304541s | *Nano Lett.* XXXX, XXX, XXX−XXX

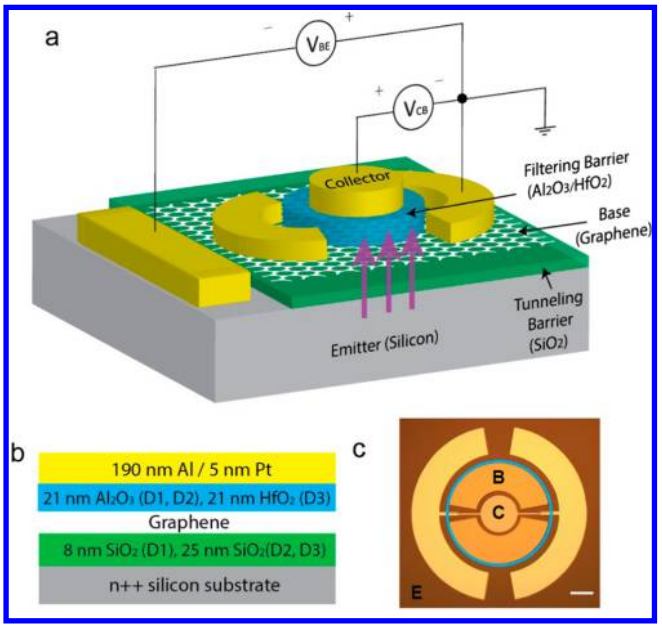

Figure 1. (a) A schematic diagram to show the collector-up GB-HET structure and the common-base configuration used to measure the $I-V$ characteristics. Graphene is used as the base region for an HET structure. The purple arrows indicate the transport direction of the hot electrons. (b) Detailed material parameters for three types of GB-HET, D1–D3. (c) Top view optical microscopy image of a GB-HET with two base contacts. The scale bar is 100 μm. Graphene is located inside the blue circle.

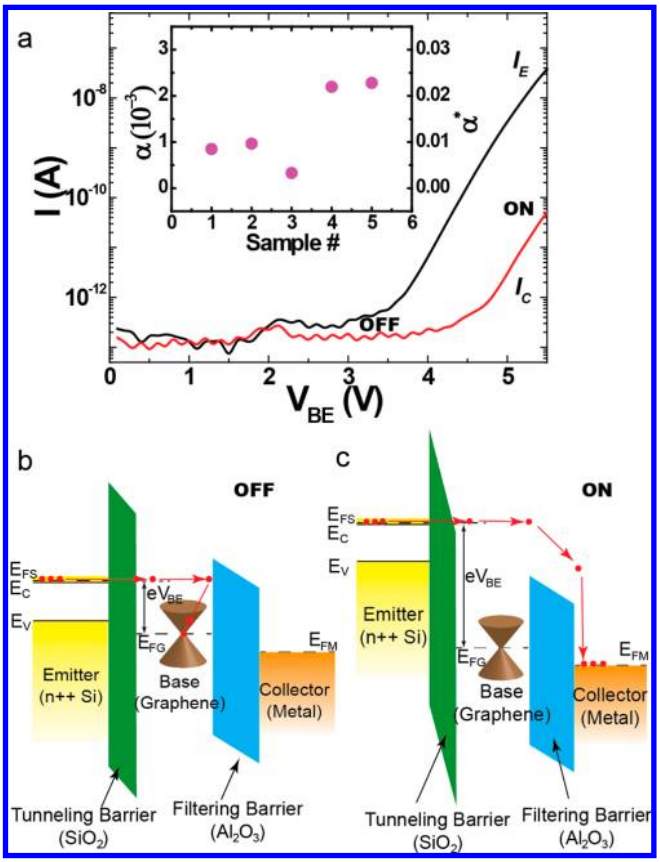

Figure 2. (a) Input and transfer characteristics of D1 at V_{CB} = 0.5 V. The device clearly exhibits distinguishable on- and off- states of the output current I_C as a function of the input voltage V_{BE}. The inset shows the common-base current gain α and the effective gain α^* for five devices with the same structure and size at V_{BE} = 5 V and V_{CB} = 0.5 V. Schematic band diagrams of D1 in the off-state (a) and on-state (b), respectively. The hot electrons tunnel from the silicon emitter to the graphene base through the SiO_2 tunneling barrier. In the-off state (a), V_{BE} is small, therefore most of the hot electrons do not have sufficient energy to travel over the filtering barrier and are bounced back into the base without contributing to the collector current I_C. In the on-state (b), V_{BE} is large enough so that hot electrons have sufficient energy to travel over the filtering barrier and reach the collector, resulting in a larger collector current I_C.

cm^{-3}). The graphene is grown on copper foil using a chemical vapor deposition (CVD) method[19,20] and then transferred onto the surface of the SiO_2/Si substrate using a poly(methyl methacrylate) (PMMA) transfer method.[21] The PMMA layer was removed with an acetone bath followed by H_2/Ar forming gas anneal at 350 °C for 1 h. Subsequently, the base contact (20 nm thick Cr/100 nm thick Au) is patterned by photolithography and deposited on graphene. The graphene outside the active region is then etched by oxygen plasma to isolate each device. The graphene area in each device is ~3.2 × 10^5 μm^2. A 2 nm thick Al seed layer is evaporated on top of graphene and naturally oxidized (i.e., $Al_{(ox)}$) in air, followed by atomic layer deposition (ALD) of a 18 nm thick Al_2O_3 as the filtering barrier. Finally, the collector (190 nm thick Al/5 nm thick Pt) and the electrodes (220 nm thick Al) are patterned and deposited on top of the filtering barrier. The effective collector area on top of graphene is ~3.5 × 10^4 μm^2. (Figure 1c)

To characterize the device performance, we first investigate the input and transfer $I-V$ characteristics of D1 under the common-base configuration, where the base is grounded (see Figure 1a). The input characteristics are specified by the dependence of the input current (I_E) on the input voltage bias (V_{BE}), while the transfer characteristics are governed by the dependence of the output current (I_C) on the input voltage bias (V_{BE}) (see Figure 2a).

An on–off ratio (I_{on}/I_{off}) of more than 10^2 for the collector current is observed, as shown in the transfer characteristics in Figure 2a. This is because the I_{on}/I_{off} in HETs primarily depends on the filtering probabilities rather than the bandgap of the channel material as in FETs. When V_{BE} is applied to the emitter, hot electrons with high kinetic energy are injected from the emitter to the base (i.e., graphene) by tunneling through the SiO_2 layer. The injected hot electrons will traverse the base region, during which some of the electrons keep their high energy and reach the base-collector filtering barrier without scattering (i.e., ballistic transport), while others lose their energy through various scattering mechanisms (e.g., phonons, electron–electron interaction, etc.). In the off-state (Figure 2b), when V_{BE} is small, the kinetic energy of most hot electrons is insufficient to overcome the filtering barrier. Hence, these electrons will be bounced back, remain in the base and eventually be collected by the base contact without contributing to the collector current I_C. In the on-state (Figure 2c), V_{BE} is large enough so that the kinetic energy of most hot electrons can overcome the filtering barrier. Therefore, a substantial fraction of the hot electrons can travel over the filtering barrier, and reach the collector, resulting in an increase of I_C. On the basis of the operation principle discussed above, an energy bandgap in the base material is not required to realize a high I_{on}/I_{off} in HETs. Therefore, the zero bandgap and semimetallic property of graphene is not a disadvantage for GB-HETs, but

dx.doi.org/10.1021/nl304541s | Nano Lett. XXXX, XXX, XXX–XXX

rather favorable for lowering the series resistance in the base region.

We also investigate the common-base output characteristics of D1, which are specified by the dependence of the output current (I_C) on the output voltage (V_{CB}). As shown in Figure 3a, I_C is mainly controlled by the input voltage V_{BE} and is not

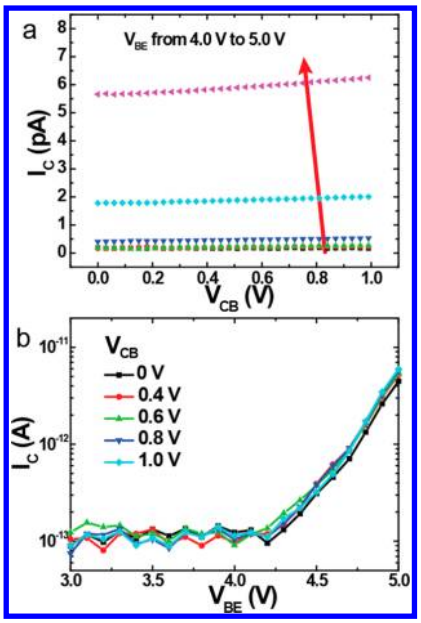

Figure 3. (a) The output $I-V$ characteristics for D1 at various V_{BE} bias. The red arrow indicates the direction of increasing V_{BE} from 4.0 to 5.0 V in steps of 0.2 V. (b) The transfer $I-V$ characteristics for D1 at various V_{CB} bias. The collector current is mainly controlled by V_{BE} rather than V_{CB}, which indicates a high-output impedance.

sensitive to the output voltage V_{CB}, which indicates a high output impedance for the device. The insensitivity of I_C to V_{CB} is corroborated by the transfer characteristics at various V_{CB} as shown in Figure 3b. This saturation behavior on I_C can be attributed to the weak dependence of the filtering barrier height on V_{CB}. As discussed above, the collector current is determined by the energy of the hot electron and the filtering barrier height. The energy of the hot electron is determined by the V_{BE} bias, while the filtering barrier height will not be significantly affected by the V_{CB} bias. As a result, the collector current is mainly controlled by V_{BE} rather than V_{CB} and a current saturation is observed.

An important figure of merit to benchmark the device performance of GB-HETs is the common-base current gain α, defined as I_C/I_E.[22] The current gain α quantifies the fraction of the injected electrons that reach the collector after suffering from various scattering and reflections in the base and at its interfaces. To separate the thermionic and hot-electron contributions in the calculation of α, we have subtracted the base/collector leakage current, given by the $I-V$ characteristic corresponding to $I_E = 0$ A,[12] from the measured collector current. The extracted α from five devices with the same structure and size as D1 range from $\sim 0.3 \times 10^{-3}$ to 2.3×10^{-3} (see the inset of Figure 2a). It is worth mentioning that the D1 GB-HET has a collector-up design in order to achieve a low collector-base capacitance for eventually a high-frequency response.[23] However, the device may suffer from a low α when the collector area is smaller than the emitter area, because only the electrons located at the small region underneath the collector contribute to the collector current. In the case of D1, the area ratio of the collector to the emitter is only ~11%, and hence an effective gain α^* (defined as α divided by the collector/emitter area ratio) is introduced to show the estimated potential practical gain if the collector is designed to have the same area as the emitter. The effective gain may be overestimated when a collector bias is applied because of the quantum capacitance of graphene.[24] The values of the effective gain α^* for the five devices range from ~0.3 to 2.1%, which are still relatively low compared to state-of-the-art HETs.[12,13]

There are two other important factors that affect the gain α (and α^*) in addition to the collector/emitter area ratio. One is the energy of hot electrons. Low-energy electrons can enter the base through undesirable channels (e.g., pin-holes) and they do not have sufficient energy to travel over the filtering barrier to reach the collector. Thus, increasing the energy of hot electrons and suppressing low-energy electrons can increase α (and α^*). The other factor is the filtering barrier height. The filtering barrier height determines the required energy for the hot electrons to reach the collector. A lower filtering barrier can increase the possibility of electrons to travel over the barrier and result in a higher α. In addition to these dominant factors that can be easily engineered, another possibility for the low α may be that the injected hot electrons in graphene may need to overcome additional energy barriers due to their transport along the direction normal to the graphene plane.[16,17,25]

On the basis of the above analysis, we have engineered and fabricated three other types of GB-HETs (i.e., D2, D3, and D4) with different structures and material parameters to improve α (and α^*). The details of the devices are given in Table 1. We

Table 1. Comparison of the Current Gain α, the Effective Gain α^*, the Current On−Off Ratio and the Parameters of Tunneling and Filtering Barriers in D1−D4

structure	tunnel barrier	filter barrier	α	α^*	on−off ratio
D1	8 nm SiO_2	21 nm Al_2O_3	0.03−0.23%	0.3−2.1%	400
D2	25 nm SiO_2	21 nm Al_2O_3	0.48−1.2%	4.4−11%	80
D3	25 nm SiO_2	21 nm HfO_2	3.7−4.8%	34−44%	300
D4	2 nm Al_2O_3	20 nm* SB	0.03%	0.03%	10^5

*The filtering barrier in D4 is the SB between graphene and Si. We use the depletion region width at $V_{CB} = 0$ V of the graphene−Si SB contact as the filtering barrier thickness.

first increase the thickness of the SiO_2 tunneling barrier from 8 to 25 nm in D2. The transfer $I-V$ characteristics of D2 at various V_{BE} are shown in Figure 4a. Compared with D1, a higher V_{BE} is required (~16 V) to observe the increase of I_C in D2 because of a thicker tunneling barrier (i.e., SiO_2). In addition, α extracted from seven devices with the same structure and size as D2 range from ~0.48 to 1.2% while the effective gain α^* range from 4.4 to 11% (see the inset of Figure 4a). The improvement of α may be attributed to the two reasons mentioned above. One is the suppression of pin-holes when the thickness of the tunneling barrier is increased. The other is that, at the same electric field, V_{BE} in D2 is larger than that in D1. As a result, the hot electrons in D2 have a higher energy than D1, allowing a larger fraction of hot electrons in D2 to travel over the filtering barrier.

Furthermore, to analyze the influence of the filtering barrier on α (and α^*), we substitute the Al_2O_3 filtering barrier layer

dx.doi.org/10.1021/nl304541s | Nano Lett. XXXX, XXX, XXX−XXX

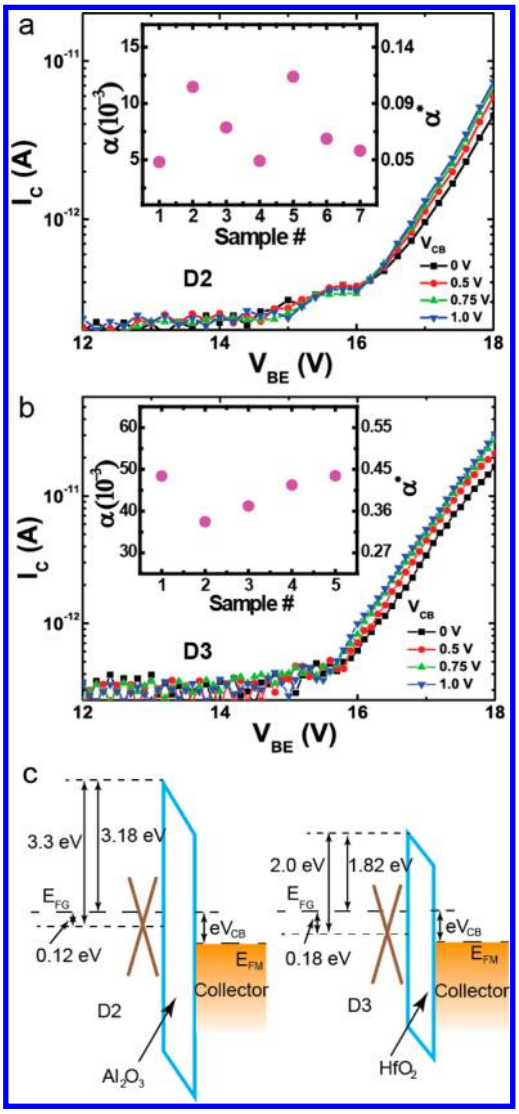

Figure 4. Transfer $I-V$ characteristics of the modified GB-HET structures, (a) D2, and (b) D3, represented in a semilogarithmic scale at various V_{CB}. The insets are the common-base current gain α and the effective gain α^* for D2 and D3, respectively. They are extracted from multiple devices with the same structure and size at V_{BE} = 18 V and V_{CB} = 0.5 V. (c) Schematic band diagrams to show the different filtering barrier heights between D2 and D3. Using HfO_2 as the filtering barrier for D3 reduces the barrier height between the Fermi level of graphene and the conduction band edge of the oxide.

with HfO_2 while maintaining the same thickness (21 nm) in D3. The transfer characteristics of D3 at various V_{BE} are shown in Figure 4b. Because the tunneling barrier is identical in D2 and D3, I_C starts to increase at similar V_{BE} (~ 16 V) in both devices. α extracted from five devices with the structure and size as D3 range from 3.7 to 4.8% and α^* range from 34 to 44% (see the inset of Figure 4b). The improvement of α (and α^*) originates from a lower filtering barrier height in D3 than D2. The lower filtering barrier height in D3 can be attributed to two reasons, as illustrated in Figure 4c. First, the band offset between the Dirac point of graphene and the conduction band edge of the HfO_2 (~2.0 eV) is lower than that of Al_2O_3 (~3.3 eV), which is determined by the work function of graphene and the electron affinity of the dielectrics.[26,27] Second, when the same V_{CB} is applied, the Fermi level shift in graphene induced by the electrostatic potential ϕ across the filtering barrier is larger in D3 than D2 because HfO_2 has a larger dielectric constant than Al_2O_3. This shift reduces the energy difference between the Fermi level of graphene and the conduction band edge of the dielectrics, resulting in a smaller filtering barrier height. To estimate this Fermi level shift in graphene for both D2 and D3, we use the equation[28]

$$V_{CB} = \frac{E_{FG}}{e} + \phi$$

with $E_{FG}/e = \hbar|V_F|(\pi n)^{1/2}/e$ being determined by the quantum capacitance of the graphene, where E_{FG} is the graphene Fermi level, $\hbar$ is the reduced Planck constant, V_F is the Fermi velocity of graphene, and n is the carrier concentration in graphene; $\phi = ne/C_F$ being determined by the geometrical capacitance $C_F = \varepsilon_0\varepsilon_{ox}/t_{ox}$ of the filtering barrier, where ε_{ox} is the dielectric constant of the filtering barrier and t_{ox} is the thickness of the filtering barrier. Since HfO_2 has a larger dielectric constant ε_{ox} than Al_2O_3,[29] the Fermi level shift in graphene is larger in D3 (~0.18 eV) compared to D2 (~0.12 eV). The two reasons discussed above both result in a lower filtering barrier height in D3. Therefore, a larger α (and α^*) is observed in D3.

In addition to the collector-up structures, D1–D3, a prototype of GB-HET with the emitter-up design (i.e., D4) is also fabricated and characterized. As shown in Supporting Information Figure S1, the collector area is larger than the emitter area in D4. Naturally oxidized Al is used as the tunneling barrier since thermal SiO_2 cannot be grown on top of graphene, metal (Ti/Au) is used as the emitter, and a graphene/silicon Schottky barrier is used as the filtering barrier. The transfer and input characteristics are shown in Figure 5.

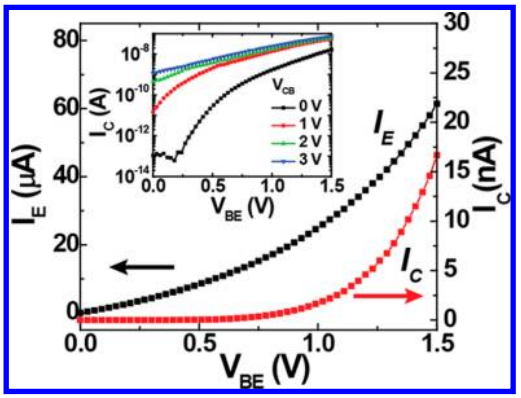

Figure 5. Transfer and input $I-V$ characteristics of the emitter-up GB-HET (D4) at V_{CB} = 0 V. D4 uses naturally oxidized aluminum as the tunneling barrier and a metal emitter. The extracted α is ~3×10^{-4} at V_{BE} = 1.5 V and V_{CB} = 0 V. The value of α is much lower than that for D1–D3 because of the undesirable pinholes in the tunneling barrier and the lack of an energy bandgap in the emitter. The inset shows the collector current in semilogarithmic scale at various V_{CB}. The highest on–off ratio (10^5) is observed when sweeping V_{BE} from 0 to 1.5 V at V_{CB} = 0.

The on-state collector current is larger in D4 compared to D1–D3 because of the thinner tunneling barrier (~2 nm) and lower filtering barrier height in D4. The highest on–off ratio (>10^5) is observed when sweeping V_{BE} from 0 to 1.5 V at V_{CB} = 0 V (the inset of Figure 5). In this case, the off-state collector current is equal to the noise level. The on–off ratio decreases as V_{CB} increases because the Schottky barrier in D4 does not provide as good an isolation as the high-k dielectrics in D1–D3.

dx.doi.org/10.1021/nl304541s | Nano Lett. XXXX, XXX, XXX–XXX

The extracted α in D4 is only $\sim 3 \times 10^{-4}$, which can be attributed to the increased contribution of low-energy carriers. First, the quality of the oxidized Al layer in D4 is not as good as the thermal SiO_2 in D1–D3, which means there are a larger portion of low-energy carriers injected into the base. Second, unlike the semiconductor emitter (i.e., n^+-Si) in D1–D3, metal (Ti/Au) is used as the emitter in D4. The addition of an energy bandgap in the semiconductor emitter for D1–D3 suppresses electrons at the valence band edge from tunneling into the graphene base, because these electrons are subject to a much higher energy barrier than those electrons located at the conduction band edge. However, there is no such effective suppression of low-energy carriers for the metal emitter in D4. Therefore, a larger portion of low-energy carriers will enter the graphene base and result in a lower α in D4.

Finally, to illustrate the effects of different device parameters, we summarize α and α^* for all of the devices (see Table 1). We note that α is considerably improved by more than 2 orders of magnitude through optimizing the device structures as well as the material parameters. This suggests the quality of the tunneling barrier and the proper choice of materials are key elements to the device performance of GB-HETs. In addition, to achieve an even higher α, the optimization of the collector-up geometrical structures (e.g., placing an isolation oxide in the emitter of D3 to confine the emitter current going only underneath the collector) should be the next step to further enhance the performance of the GB-HET.

In conclusion, we have demonstrated and compared four types of vertical GB-HETs with a variety of structures and material parameters. Benefiting from the non-FET concept, a high current on–off ratio of over 10^5 is achieved. The common-base current gain α is significantly improved by modifying the device structures and the material parameters (e.g., a usage of thermal SiO_2 as the tunneling barrier, a thicker tunneling barrier, an introduction of the energy bandgap in the emitter, and a reduced filtering-barrier height). In spite of the smaller collector/emitter area ratio (~11%), a moderate value of α (~4.8%) and α^* (~44%) is achieved in our device. Our devices illustrate the potential of GB-HETs as an alternative route to utilize the unique properties of graphene, such as the single-atomic thickness and the semimetallic property without suffering from the zero bandgap of graphene or the mobility degradation of graphene nanoribbons.[30,31] Through further optimization, a high gain and a short transit time can be achieved based on the present structures. These results suggest the potential of GB-HETs for future high-speed electronic device applications.

■ ASSOCIATED CONTENT

Supporting Information

The emitter current for D1–D3, the leakage current for D1–D3, the common-emitter output characteristics for D1, the I–V characteristics for the devices with broken dielectrics, the structure and fabrication processes for D4, the Schottky contact between graphene and silicon, and the output characteristics for D4. This material is available free of charge via the Internet at http://pubs.acs.org.

■ AUTHOR INFORMATION

Corresponding Author

*E-mail: wang@ee.ucla.edu.

Notes

The authors declare no competing financial interest.

■ ACKNOWLEDGMENTS

This work is supported by the Focus Center Research Program (FCRP) - Functional Engineered Nano Architectonics (FENA).

■ REFERENCES

(1) Bolotin, K. I.; Sikes, K. J.; Hone, J.; Stormer, H. L.; Kim, P. *Phys. Rev. Lett.* **2008**, *101* (9), 096802.
(2) Li, X.; Cai, W.; An, J.; Kim, S.; Nah, J.; Yang, D.; Piner, R.; Velamakanni, A.; Jung, I.; Tutuc, E.; Banerjee, S. K.; Colombo, L.; Ruoff, R. S. *Science* **2009**, *324* (5932), 1312–1314.
(3) Novoselov, K. S.; Geim, A. K.; Morozov, S. V.; Jiang, D.; Zhang, Y.; Dubonos, S. V.; Grigorieva, I. V.; Firsov, A. A. *Science* **2004**, *306* (5696), 666–669.
(4) Liao, L.; Lin, Y.-C.; Bao, M.; Cheng, R.; Bai, J.; Liu, Y.; Qu, Y.; Wang, K. L.; Huang, Y.; Duan, X. *Nature* **2010**, *467* (7313), 305–308.
(5) Wu, Y.; Lin, Y.-m.; Bol, A. A.; Jenkins, K. A.; Xia, F.; Farmer, D. B.; Zhu, Y.; Avouris, P. *Nature* **2011**, *472* (7341), 74–78.
(6) Chen, J.-H.; Jang, C.; Xiao, S.; Ishigami, M.; Fuhrer, M. S. *Nat. Nanotechnol.* **2008**, *3* (4), 206–209.
(7) Chen, J. H.; Jang, C.; Adam, S.; Fuhrer, M. S.; Williams, E. D.; Ishigami, M. *Nat. Phys.* **2008**, *4* (5), 377–381.
(8) Schwierz, F. *Nat. Nanotechnol.* **2010**, *5* (7), 487–496.
(9) Mead, C. A. In *The Tunnel-Emission Amplifier*; Proceedings of the Institute of Radio Engineers; Institute of Radio Engineers: New York, 1960; Vol. *48*, Issue 3, pp 359–361.
(10) Shannon, J. M. *IEE J. Solid-State Electron Devices* **1979**, *3* (5), 142–144.
(11) Heiblum, M.; Thomas, D. C.; Knoedler, C. M.; Nathan, M. I. *Surf. Sci.* **1986**, *174* (1–3), 478–480.
(12) Moise, T. S.; Kao, Y. C.; Seabaugh, A. C. *Appl. Phys. Lett.* **1994**, *64* (9), 1138–1140.
(13) Evers, N.; Laskar, J.; Jokerst, N. M.; Moise, T. S.; Kao, Y. C. *Appl. Phys. Lett.* **1997**, *70* (18), 2452–2454.
(14) Heiblum, M. *Solid-State Electron.* **1981**, *24* (4), 343–366.
(15) Heiblum, M. *Solid-State Electron.* **1988**, *31* (3–4), 617–618.
(16) Mehr, W.; Dabrowski, J.; Scheytt, J. C.; Lippert, G.; Xie, Y.-H..; Lemme, M. C.; Ostling, M.; Lupina, G. *IEEE Electron Device Lett.* **2012**, *33* (5), 691–693.
(17) Kong, B. D.; Zeng, C.; Gaskill, D. K.; Wang, K. L.; Kim, K. W. *Appl. Phys. Lett.* **2012**, *101* (26), 263112.
(18) Vaziri, S.; Lupina, G.; Henkel, C.; Smith, A. D.; Ostling, M.; Dabrowski, J.; Lippert, G.; Mehr, W.; Lemme, M. C. *Nano Lett.* **2013**, *13* (4), 1435–1439.
(19) Rasool, H. I.; Song, E. B.; Allen, M. J.; Wassei, J. K.; Kaner, R. B.; Wang, K. L.; Weiller, B. H.; Gimzewski, J. K. *Nano Lett.* **2010**, *11* (1), 251–256.
(20) Rasool, H. I.; Song, E. B.; Mecklenburg, M.; Regan, B. C.; Wang, K. L.; Weiller, B. H.; Gimzewski, J. K. *J. Am. Chem. Soc.* **2011**, *133* (32), 12536–12543.
(21) Suk, J. W.; Kitt, A.; Magnuson, C. W.; Hao, Y.; Ahmed, S.; An, J.; Swan, A. K.; Goldberg, B. B.; Ruoff, R. S. *ACS Nano* **2011**, *5* (9), 6916–6924.
(22) Heiblum, M.; Fischetti, M. V. *IBM J. Res. Dev.* **1990**, *34* (4), 530–549.
(23) Gruhle, A.; Kibbel, H.; Mahner, C.; Mroczek, W. *IEEE Trans. Electron Devices* **1999**, *46* (7), 1510–1513.
(24) The quantum capacitance of graphene induces a Fermi level shift in graphene. This reduces the band offset between SiO_2 and the graphene base, resulting in an increased current density inside the area covered by the collector as compared to the area not covered by the collector.
(25) Wallace, P. R. *Phys. Rev.* **1947**, *71* (9), 622–634.
(26) Robertson, J. *J. Vac. Sci. Technol. B* **2000**, *18* (3), 1785–1791.

(27) Yu, Y.-J.; Zhao, Y.; Ryu, S.; Brus, L. E.; Kim, K. S.; Kim, P. *Nano Lett.* **2009**, *9* (10), 3430−3434.
(28) Das, A.; Pisana, S.; Chakraborty, B.; Piscanec, S.; Saha, S. K.; Waghmare, U. V.; Novoselov, K. S.; Krishnamurthy, H. R.; Geim, A. K.; Ferrari, A. C.; Sood, A. K. *Nat. Nanotechnol.* **2008**, *3* (4), 210−215.
(29) Osburn, C. M.; Kim, I.; Han, S. K.; De, I.; Yee, K. F.; Gannavaram, S.; Lee, S. J.; Lee, C. H.; Luo, Z. J.; Zhu, W.; Hauser, J. R.; Kwong, D. L.; Lucovsky, G.; Ma, T. P.; Ozturk, M. C. *IBM J. Res. Dev.* **2002**, *46* (2.3), 299−315.
(30) Han, M. Y.; Ozyilmaz, B.; Zhang, Y.; Kim, P. *Phys. Rev. Lett.* **2007**, *98* (20), 206805.
(31) Li, X.; Wang, X.; Zhang, L.; Lee, S.; Dai, H. *Science* **2008**, *319* (5867), 1229−1232.